ACS APPLIED MATERIALS & INTERFACES

Research Article

www.acsami.org

Hollow Microgel Based Ultrathin Thermoresponsive Membranes for Separation, Synthesis, and Catalytic Applications

Bijay Prakash Tripathi,*[,†] Nidhi Chandrama Dubey,[†,‡] and Manfred Stamm*[,†,‡]

[†]Leibniz-Institut für Polymerforschung Dresden e.V., Hohe Straße 6, 01069 Dresden, Germany

[‡]Physical Chemistry of Polymer Materials, Technische Universität Dresden, 01069 Dresden, Germany

Supporting Information

ABSTRACT: Thermoresponsive core−shell microgels with degradable core are synthesized via surfactant based free radical polymerization using N,N′-(1,2-dihydroxyethylene)bis(acrylamide) (DHEA) as a cross-linker for core preparation. The 1,2-glycol bond present in DHEA is susceptible to $NaIO_4$ solution, and thus, the structure can be cleaved off resulting in hollow microgel. Ultrathin membranes are prepared by suction filtration of a dilute suspension of core−shell microgels over a sacrificial layer of $Cd(OH)_2$ nanostrand coated on track etched membrane. After removal of the degraded cores from microgels, the membranes are cross-linked with glutaraldehyde and the nanostrands are removed by passing a 10 mM HCl solution. The prepared membranes are thoroughly characterized using scanning electron microscopy (SEM), atomic force microscopy (AFM), dynamic light scattering (DLS), and dynamic contact angle for morphology, thermoresponsive, and hydrophilic properties, respectively. The prepared membranes showed thermoresponsive permeation behavior and remarkable separation performance for low molecular weight dyes and lysozyme protein. These membranes are also used to synthesize gold nanoparticles and immobilize lactate dehydrogenase enzyme for catalytic and biocatalytic application. The results for water permeation, solute rejection, and ability to immobilize gold nanoparticles and enzymes showed its wide range of applicability. Furthermore, the synthesis of hollow microgel is simple and environmentally friendly, and the membrane preparation is easy, scalable, and other microgel systems can also be used. These responsive membranes constitute a significant contribution to advanced separation technology.

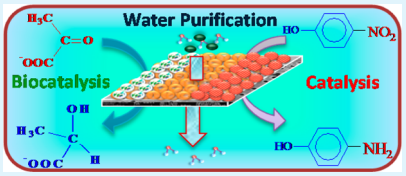

KEYWORDS: *hollow microgel, ultrathin microgel membrane, thermoresponsive membrane, separation, catalytic applications*

INTRODUCTION

Microgels are internally cross-linked micrometer or sub micrometer sized soft responsive particles made of hydrophilic cross-linked polymers swollen by solvent.[1] Being soft in nature, the microgel particles can be both compressed and deformed to a large degree based on cross-linking density and polymer−solvent interaction of their constituent polymer network.[2,3] The degree of swelling of these microgel particles can be controlled by changing the cross-linking density, the chemical nature of the monomer, or by the incorporation of suitable comonomer. The swelling of these microgels can be tuned by external stimuli such as pH, temperature, ionic strength, etc.[4] Microgels composed of environmentally responsive polymers continue to attract attention due to their potential applications in numerous fields, including drug delivery, chemical separations, sensors, and catalysis.[4−11]

PNIPAm is perhaps the most widely studied polymer for the synthesis of microgels due to its unique thermoresponsive and hydrophilic nature.[5,12] In aqueous media, PNIPAm exhibits a lower critical solution temperature (LCST) at about 32 °C.[13] Below the LCST, PNIPAm is fully soluble in water due to the formation of hydrogen bonds between water molecules and the amide side chains. With the increase in solution temperature, the polymer undergoes a "coil-to-globule" phase transition due to disruption of these hydrogen bonds, as well as the release of structured water around the isopropyl groups.[13,14] The release of bonded water molecules entropically favored hydrophobic aggregation of the polymer, which leads to globule formation.[14] In the case of microgels, this transition is called a volume phase transition (VPT), since the dissociated water molecules are expelled from the microgel interior, thus causing a decrease in volume above the LCST of the polymer.[5,6] Above properties of these materials makes them attractive in diversified applications ranging from coatings, immobilization, cell adhesion, film formation, self-healing films, etc.[3,8,15]

The hydrophilic nature of these microgels makes them potential antifouling and protein resistant coatings. Nolan et al. investigated the performance of PNIPAm microgels cross-linked by short poly(ethylene glycol) (PEG) chains, as protein adsorption-resistant films.[16] The results indicated that glass surfaces coated with microgels showed reduced protein adsorption and cell adhesion in vitro (i.e., nonfouling behavior). Microgel coatings can also be used to immobilize bactericidal agents such as nanoparticles to fabricate antibacterial surfaces. Schwartz et al. reported antimicrobial composite materials incorporating zinc oxide nanoparticles into the biocompatible PNIPAm hydrogel layers prepared by mixing of PNIPAm prepolymer with zinc oxide nanoparticles, followed by spin-

Received: June 25, 2014
Accepted: September 17, 2014
Published: October 1, 2014

   dx.doi.org/10.1021/am504120c | ACS Appl. Mater. Interfaces 2014, 6, 17702−17712

coating and photo cross-linking.[17] These materials can be used for thin membrane fabrication due to their strong cross-linking ability, film formation, and stable thin coating layer on support. There are reports available where microgel films were used as membranes.[18−21] Microgel based membranes have the added advantage of high water content in their structure, thereby reducing the adsorption of nonspecific protein binding to the membrane, and thus reducing the effects of fouling. The major problem with microgel films is the poor mechanical stability, and for such membranes to be used in filtration devices, they can be grafted within the pores of porous membranes,[22,23] physically blended with other polymers (e.g., polysaccharides),[24,25] formed in situ by encapsulating a porous membrane support[26,27] or supported on membranes.[18,28] In all above studies, the membranes were made by either modification of pores or surfaces with microgels. Thus, the membrane properties largely depended upon the properties of support membranes. Modification of the membrane support with microgels increases the effective thickness and thus the total resistance to permeation. The permeation theory predicts that the filtration rate is proportional to the pressure difference across the filtration membrane and inversely proportional to the thickness of the membrane.[29] Thus, ultrathin and stable separation layers are required for low pressure and high permeation rate membranes.

Here, we report on a new type of ultrathin filtration membranes made of cross-linked hollow microgels. The hollow microgels were obtained by removal of the core from microgels with core−shell structure. These hollow microgels were suction filtered on polyethylene terephthalate track etched membranes over $Cd(OH)_2$ nanostrands. Removal of sacrificial layer and cross-linking of the microgels led to the formation of ultrathin porous membranes. The prepared membranes were well characterized for their structure, morphology, and physical properties. These membranes were then tested for water permeation, dye and protein rejection, gold nanoparticle synthesis, catalytic behavior, and enzyme immobilization for biochemical reactions. The results indicate that these types of membranes can be used for many applications.

EXPERIMENTAL SECTION

Materials. All chemicals were purchased from Aldrich unless otherwise stated. N-isopropylacrylamide (97%, NIPAm) was purified by recrystallization in *n*-hexane before use. N,N′-(1,2-dihydroxyethylene)bis(acrylamide) (DHEA), N,N′-methylene bis(acrylamide) (≥99.5%) (BIS), sodium dodecyl sulfate (SDS), cadmium chloride, and ethanolamine were used as received. The polyethylene terephthalate track etched microporous membranes (diameter = 47 mm, pore size = 0.3−0.4 μm, pore density = 1.5×10^8 pores/cm^2) were obtained from it4ip, Belgium. Deionized (DI) water and water purified with a Milli-Q system (Millipore) were used in this study.

Synthesis of Core−Shell Microgel. The core and core−shell microgel particles were synthesized by surfactant assisted free radical precipitation polymerization under Argon atmosphere. The PNIPAm-DHEA microgel cores were prepared by the methodology described elsewhere.[30] Briefly, the monomers (NIPAm = 711 mg, DHEA = 140 mg) and surfactant SDS (44 mg) were introduced to deoxygenated water (100 mL). The mixture was then stirred and bubbled with Argon at 70 °C for 2 h. The polymerization was initiated with the addition of initiator ammonium per sulfate (APS) and reaction was allowed to continue under similar conditions for 4 h. The PNIPAm-DHEA microgel particles were further used as seed for the synthesis of core−shell microgel. The seed solution (20 mL) in the presence of SDS surfactant (20 mg) was degassed. whereas solution of NIPAm (400 mg), BIS (13.6 mg), and APMA (10 mg) were prepared separately and degassed with Argon at room temperature and finally added to the heated seed solution. The initiator APS (34 mg) dissolved separately was added to initiate the polymerization and formation of the shell. After completion of the reaction, the solution was cooled and filtered to remove any aggregate formed. Finally, the synthesized core−shell microgel particles were dialyzed for a week using 14 kDa MWCO dialysis tube (Sigma-Aldrich) against daily change of water to remove unreacted monomers and oligomers.

The core of the core−shell microgels was degraded with sodium periodate solution. A molar $NaIO_4$ solution was added in the microgel solution under stirring and allowed to react for overnight. The amount of $NaIO_4$ required was calculated based on the amount of DHEA present in microgel.

Microgel Characterizations. Dynamic light scattering (DLS) measurements of the prepared core, core−shell, and microgel with degraded core was performed under varying temperature to investigate the particle size and their thermoresponsive characteristics. DLS was carried out using Zeta sizer Nano 3000HS (Malvern Instruments, U.K.), equipped with a 633 nm He/Ne laser and a noninvasive back scatter (NIBS) technology. All samples were thermally equilibrated for 5 min and data were acquired by averaging 30 measurements, with a 10 s integrating time for each measurement. Volume phase transition temperature was determined with respect to temperature (24 to 40 °C).

Microgels morphology in dry state was investigated by scanning electron microscopy (SEM) and atomic force microscopy (AFM) characterization. The imaging was performed using a NEON 40 FIB-SEM workstation (Carl Zeiss AG, Germany) operated at 3 kV, after 3 nm thick sputter coating of platinum. The AFM imaging was performed by a Dimension 3100 (Nanoscope IV Controller; Veeco/Digital Instruments, Santa Barbara, CA) scanning force microscope in the tapping mode. The tip characteristics are as follows: spring constant 1.5−3.7 N m^{-1}, resonant frequency 45−65 kHz, tip radius about 10 nm. The dilute microgel suspensions were spin coated on a silicon wafer and dried with N_2 gas at room temperature.

Membrane Fabrication. *Preparation of Cadmium Hydroxide Nanostrands.* The cadmium hydroxide nanostrand were prepared by the procedure described elsewhere.[31] Briefly, an aqueous solution of 4 mM cadmium nitrate was mixed with an equal volume of 0.3 mM 2-aminoethanol under vigorous stirring, followed by aging for 30 min. The nanostrands spontaneously formed in the solution were used without any further treatment.

Fabrication Process of Ultrathin Microgel Membrane. The hollow microgel based membranes were fabricated on polyethylene terephthalate track etched membrane support. The membrane fabrication was carried out in a suction filtration setup. To avoid the clogging of track etched pores, 10 mL nanostrands solution was suction filtered on PET membrane placed on glass filter holder. Subsequently, a given volume (1 mL, 2 mL, and 3 mL) of core−shell microgel solution (2 mg/mL) was suction filtered. The microgels were then cross-linked by filtering 5 wt % aqueous glutaraldehyde solution for 10 min. To degrade the core, molar solution of sodium periodate was added to the filtration funnel and left for overnight under low suction pressure. The suction pressure was applied so that the sodium periodate solution can penetrate into the film. After degradation of core, large amount of water was filtered through the film to remove the degraded core. Finally, 10 mL of 10 mM HCl solution was passed to remove sacrificial nanostrand layers. Thus, obtained thin microgel film was used for all practical purposes.

Membrane Characterizations. Surface and cross-section morphology of the membranes were investigated by SEM. Hydrophilic property was characterized in terms of water absorption and contact angle measurements. For water absorption study, membrane samples with known dry weight were immersed in deionized water for 6 h at room temperature and at 45 °C. The wet sample weight was recorded, and the water absorption capacity was calculated.[32]

Application of Prepared Ultrathin Microgel Membranes. The prepared membranes were used for different applications due to their diverse characteristics. The detail experimental conditions are listed below.

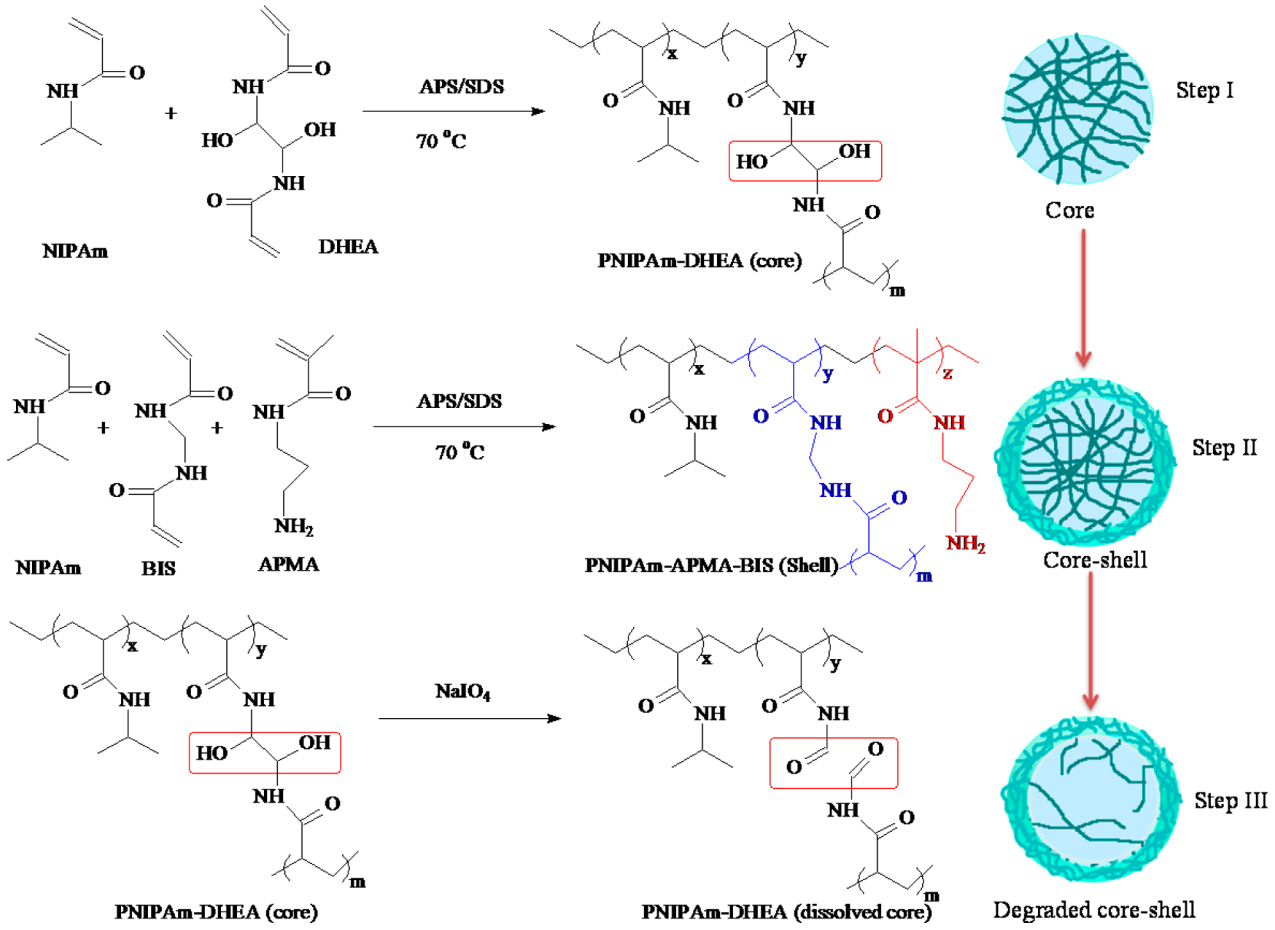

Figure 1. Reaction schemes for stepwise synthesis of core (I), core−shell (II), and dissolved core−shell (III) microgels. The schematic pictures show the different state of microgels.

Water Purification Applications. A dead-end stirred cell filtration device (Amicon 8010) connected with a nitrogen gas cylinder and solution reservoir was designed to characterize for pure water flux, solute rejection, fouling, and flux recovery ability of the membranes. Measurement of water flux was carried out at different pressures ranging from 1 to 3 bar. Each membrane was initially pressurized at 4 bar for 15 min; then, the pressure was set to the certain operating pressure from 1 to 3 bar. The water flux (J_w (L m^{-2} h^{-1})) was defined as

$$J_w = V/A\Delta t \quad (1)$$

where V (L) was the volume of permeated water, A (m^2) was the effective membrane area, and Δt (h) was the permeation time. The actual filtration area of our filtration setup is 3.8687 cm^2, and the effective filtration area of the membranes were calculated based on the porosity data obtained by counting of pores in SEM image and measuring the radius of pore. We calculated 1.5 × 10^8 pores cm^{-2} and 300 nm radius of PET track etched membranes. Thus, the effective membrane area was found to be 1.6399 cm^2. This area value was used in all flux related calculations.

Dye and Protein Rejection Application. The rejection performance of developed membranes was assessed for different molecular weight charged dyes. A 5 mg L^{-1} dye solution (methylene blue, methyl red, and congo red) was filtered at 3 bar trans-membrane pressure and the percent rejection was calculated according to the following equation:

$$\text{Rejection (\%)} = \left(1 - \frac{C_p}{C_f}\right)100 \quad (2)$$

where C_p and C_f are permeate and feed concentrations of dyes, respectively. Vigorous stirring of the solution (>300 rpm) minimized the concentration polarization at the membrane surface. The experiment was repeated three times and permeates was collected. The concentration of dye in solution was obtained by recording UV−vis spectra. Similarly, the rejection of a model protein (lysozyme; 1 mg/mL) was also studied and concentration was recorded with the help of UV−vis spectra.

Water flux recovery after the filtration of dye and protein solutions was recorded to assess the antifouling ability of the prepared membranes. The flux recovery was calculated using the following equation:

$$\text{Flux recovery (FR, \%)} = \frac{J_v}{J_w}100 \quad (3)$$

where J_w is the pure water flux of sample membrane before fouling and J_v is the pure water flux after fouling. The higher value of FR is an indicator of the better antifouling property of the membranes.

Catalytic Application. Gold nanoparticles were synthesized inside the shell of hollow microgels for catalytic applications according to the procedure published elsewhere.[33] In brief, 1 mL of 6.5 mM aqueous solution of $HAuCl_4$ was mixed with 2.5 mL of 1 mg/mL microgel dispersion at pH 6. The $HAuCl_4$ in the mixture was reduced by 10 mL of 8.8 mM $NaBH_4$ to yield a ruby-red dispersion. The gold nanoparticles/microgel complex was purified by a centrifugation-redispersion process three times to remove unreacted substances. Similarly, the gold nanoparticles were also synthesized in the membrane. After the formation of a thin hollow microgel layer desired amount of $HAuCl_4$ solution was slowly filtered through the film to allow the uptake of gold inside the microgels. Aqueous $NaBH_4$ solution was then passed to form the gold nanoparticle. The reduction of *p*-nitrophenol was carried out in UV cuvette in the presence of gold

nanoparticles loaded microgels. The reaction mixture was made by mixing of 0.1 mL of 2 mM *p*-nitrophenol with 1 mL of 0.03 M $NaBH_4$ solution and 1.9-*x* mL of water (where *x* is the volume of aqueous MG-GNP solution; 25, 50, 75, and 100 μL) in a 3 mL standard quartz cuvette (path length 1 cm). To this reaction mixture, different amount of gold nanoparticle loaded microgels (diluted to 0.025 mg/mL from initial 1 mg/mL core−shell microgel) was added. The reduction was monitored by UV−vis spectroscopy (Specord 40, Jena, Germany) after every 60 s. The conversion was also studied in stirred cell under 3 bar applied pressure in the presence of $NaBH_4$ with relatively high concentration of *p*-nitrophenol. The feed solution (1.7 mL of water/0.3 mL of 2 mM solution of *p*-nitrophenol/1 mL of 0.03 M $NaBH_4$) was fed into the Millipore stirred cell with gold nanoparticle-microgel membrane and reduction was monitored under different applied pressure to control the permeate flux. Permeate was collected at different fluxes (or applied pressure) to allow the different residence time of reactants in the membrane. The decay in absorbance for *p*-nitrophenol was recorded by UV−vis absorbance spectroscopy. To evaluate the long-term stability and reusability of the membrane, the catalytic reduction was also performed for 10 consecutive cycles with proper washing after each cycle.

Biocatalytic Application. Responsive microgels are believed to be a good enzyme immobilizing substrate. In the present study, we investigated the covalent immobilization of lactate dehydrogenase enzyme (LDH) and its biocatlytic efficiency and reusability. A relatively thin membrane than MG-3 with 0.5 mg/mL microgel solution was fabricated for enzyme immobilization study. After microgel film formation and cross-linking with glutaraldehyde, LDH solution (0.5 mg/mL) was poured on to the surface of membrane and allowed for the covalent attachment with free aldehyde groups. After a certain time interval, the solution was filtered and the surface was washed to remove uncross linked LDH from the membrane. The immobilization of enzyme was calculated by recording the concentrations of LDH in permeate and wash using the following equation:

$$\text{Enzyme immobilization } (\mu g/cm^2) = \frac{E_f - E_w}{A} \quad (4)$$

where E_f and E_w are the amount of LDH in feed and in wash, respectively. *A* is the area of membrane used for immobilization.

The conversion of pyruvate to lactate was indirectly monitored by recording the disappearance of NADH absorbance peak at 340 nm in spectrophotometer. In this case, the rate of the enzymatic reaction converting pyruvate into lactate will be equal to the rate of conversion of NADH into NAD^+. The reaction assay was composed of 1 mM pyruvate and 1 mM NADH in 100 mM TrisCl buffer pH (pH 8). The reusability test was performed on the same membrane for three consecutive cycles of operation.

RESULTS AND DISCUSSION

Soft hollow microgel based nanostructured membranes with easy and straightforward fabrication strategy were prepared over track etched support. First, the hollow microgel particles were synthesized by removing degradable core from core−shell microgels. The hollow microgels were suction filtered and cross-linked with glutaraldehyde to obtain a thin layer upon PET track etched membrane. The prepared membranes were used for water filtration, rejection of dye and proteins, in situ gold nanoparticle synthesis for chemical catalysis, and enzyme immobilization for biocatalytic applications.

Microgel Synthesis. The core−shell microgels were prepared by two stage free radical precipitation polymerization and the scheme for the reaction is presented in Figure 1. In the first step, degradable PNIPAm core was synthesized using N,N′-(1,2-dihydroxyethylene)bis(acrylamide) (DHEA) as a cross-linker. In the second step, the shell was synthesized using PNIPAm-DHEA microgel as the seed and polymerization were carried in the presence of cross-linker bis-acrylamide and functional comonomer APMA. The APMA was used in the shell synthesis to include free amine groups for covalent cross-linking with glutaraldehyde and further particle immobilization. After the formation of core−shell structure, the degradation of the core was performed using $NaIO_4$ and the photographs of core−shell and core dissolved microgel solutions are given in Figure S1 (Supporting Information). The core dissolved microgel suspension showed a more clear solution than the core−shell microgel. The DHEA monomer contains a vicinal diol functionality, which can be easily cleaved by the stoichiometric amount of $NaIO_4$. The clear solution after $NaIO_4$ addition and washing under centrifugation showed that, 1,2-glycol bond was successfully cleaved, which resulted in the formation of smaller polymer segments. These polymer segments were removed by proper washing by centrifugation-redispersion process.

PNIPAm exhibits a reversible phase transition from a solvated random coil to a desolvated globular state at around 32 °C, this is due to the disruption of hydrogen bonds and the dominance of hydrophobic part of PNIPAm at high temperature, causing entropically favored removal of water.[6,14] The microgels possess a volume phase transition (VPT) from a swollen state to a collapsed state at or near this temperature. Furthermore, this transition temperature is also affected by the presence of functional comonomer in the structure.[34,35] The change in hydrodynamic diameter of the core, core−shell, and core dissolved microgel particles with respect to temperature was studied by DLS. From Figure S2 (Supporting Information), it was observed that the synthesized microgels exhibit phase transition at around 32 °C, which is near to the LCST of PNIPAm. The size of core, core−shell, and core dissolved microgels in water at 24 °C was found to be 431, 586, and 765 nm, while at 40 °C, the size reduced to 148, 365, and 327 nm, respectively. Below the LCST of PNIPAm, the hydrodynamic diameter of the core dissolved microgels was found to be higher, whereas above the LCST, the size was smaller compared to the core−shell microgel. The macromolecules (PNIPAm) and their concentration play crucial role in hydration of gel and diffusion of water molecule during the phase transition.[14] In the microgels with dissolved core the reduced number of PNIPAm chains allows more hydration of shell compared to the core−shell microgels. In addition to this, during the synthesis of core−shell particles, interpenetrating network is formed at the interface of the core and the shell, and thus, the core has a significant effect on the swelling behavior of the shell. Following the dissolution of the core, the shell is freed from the constraint of dense core, leading to a higher intrinsic swelling capacity of hollow microgel compare to that of core−shell microgel. Due to this, microgels with dissolved core also possess sharper phase transition and smaller swelling volume at high temperatures than the core−shell particles. This result indicates that the number of cross-linking sites was reduced in core dissolved sample, which allows the microgel shell to swell and shrink to a greater extent.[30] The morphology of core−shell and core dissolved microgels deposited on silicon wafer was observed with the help of SEM and AFM imaging. The images are depicted in Figure S3 (Supporting Information). Both SEM and AFM images clearly revealed that the microgels were of nearly uniform size and their morphology was retained after core degradation. The core degradation and their removal are clearly visible in the AFM image. The size of the hollow microgels in the AFM image was larger than in the SEM image.

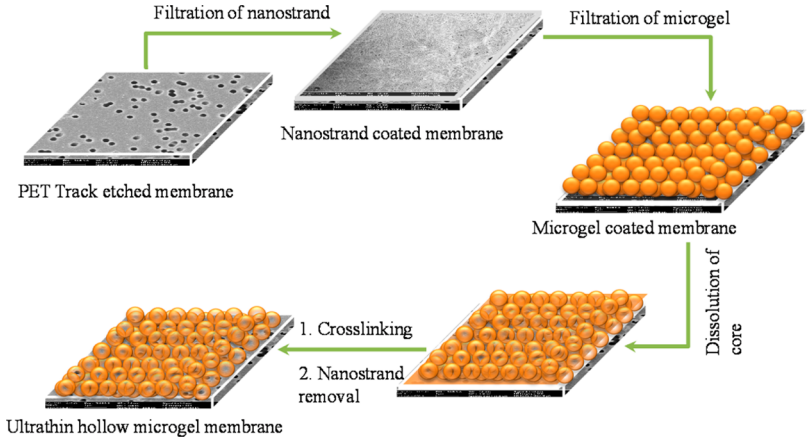

Figure 2. Fabrication process of ultrathin cross-linked hollow microgel membrane.

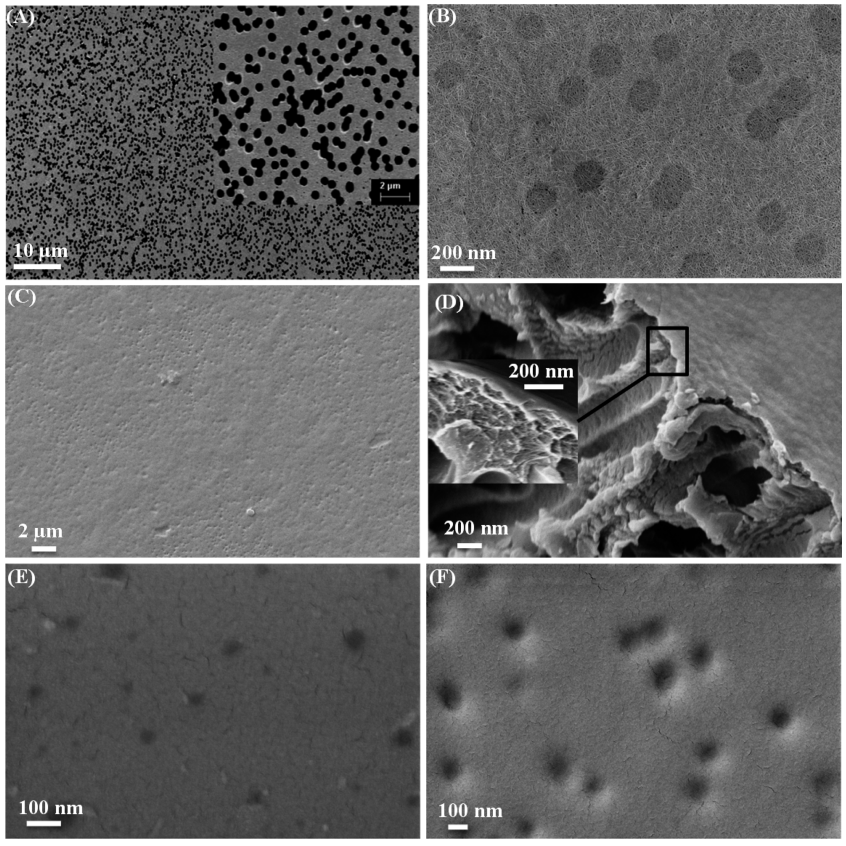

Figure 3. Scanning electron microscopy images of different membranes: (A) PET; (B) $Cd(OH)_2$ nanostrand coated PET; (C) microgel film on PET; (D) cross-section of microgel deposited PET (the inset image is showing high resolution of microgel layer); (E) microgel deposited PET before nanostrand removal; and (F) microgel deposited PET after nanostrand removal.

This can be explained due to the presence of water in samples used for AFM imaging, whereas for SEM imaging, the samples were completely dry. The AFM images also indicate that the size of the core dissolved microgel particles size was larger than the size of core−shell microgel particles. This can be attributed to the loss of inter cross-linked nature between core and shell as well as due to the high water absorption. Similar trends were also obtained in DLS characterizations.

Membrane Fabrication and Characterization. Packing of soft deformable microgel colloids by external compression transforms a suspension of loose microgel particles into an arrested state with properties similar to that of a macroscopic gel.[3] In this study also, the loose hollow microgel suspension was transformed into ultrathin cross-linked film under suction filtration condition. The stepwise membrane fabrication process is given in Figure 2. The membranes were prepared by a simple suction filtration process on $Cd(OH)_2$ nanostrand covered PET track etched membranes. The sacrificial nanostrand layer prevents the intrusion of microgels into the pores of track etched membranes. After suction filtration of microgel solutions, cross-linking was carried out by slowly passing the glutaraldehyde solution. Amino groups of APMA moieties allow the covalent cross-linking of microgel particles together. After cross-linking of microgels, $NaIO_4$ solution was poured on

membranes fitted into the suction filtration assembly under low suction pressure. After certain time interval, the $NaIO_4$ solution was filtered out and membranes were washed with copious amount of water until constant water permeation was reached for a given volume of water. The membrane fabrication strategy is simple and straightforward which can be easily scaled up depending upon the porous support, suction filtration assembly, as well as the direct control over thickness by varying the volume and concentration of microgel solution.

Morphology of the thin microgel film was characterized by SEM microscopy, and the images are presented in Figure 3. The porous structure of the PET membrane and finely covered pores are clearly visible in Figure 3(A and B). The image also indicates that the nanostrand layer was quite thin and uniformly covered the PET membrane. Figure 3(C and D) shows the surface and cross-section images of microgel layers deposited on sacrificial nanostrand layer. The smoothly deposited thin layer of microgels reflects the formation of homogeneous and uniform membrane. After cross-linking, degradation, and removal of nanostrand layer, the microgel thin film was slightly dented and curved grooves were formed. However, this deformation was less observed in thicker films. Also, the pores of PET membrane were intact and no clogging was observed in the cross-section image. The cross-section images (Figure 3D and high resolution inset image) clearly indicate that the pores of the PET membrane were intact and no blockage was observed. Also, the effective thickness of deposited and cross-linked microgel layer was ~450 nm, which indicate that the microgel film constitute an ultrathin membrane over PET support. Moreover, no cracks, holes, and deformations were observed on the membrane surface.

The hydrophilic properties of microgel membranes were characterized by recording the water absorption behavior and dynamic contact angle values on surfaces. The components of microgel (PNIPAm and APMA) are hydrophilic in nature and tend to absorb large amounts of water at room temperature. Upon immersing the membranes in water, the PNIPAm chains are expected to swell at temperatures below its coil−globule transition temperature. However, the glutaraldehyde cross-linking of APMA block could dampen the extent of water absorption. At the temperature beyond transition temperature, the PNIPAm chains are expected to become hydrophobic due to conformational collapse and reduce the absorption of water. The water uptake for the membranes at room temperature (RT) and 45 °C are given in Table S1 (Supporting Information). The water content at RT was found to increase with the microgel content in the membrane. At 45 °C, the water absorption was quite low as compared to RT, and also, very small changes were observed with increasing amount of microgel in the membrane. The contact angle values recorded at RT, for all membranes, are also included in Table S1. The data reveal that the membranes were hydrophilic in nature and a decrease in contact angles was observed with increasing thickness of the membrane. This phenomenon can be explained due to the availability of a high number of polar and hydrophilic groups on the surface and fast absorption of water. The solid−liquid interaction free energy resulting from interactions between the solid surface and the applied water molecules was derived from contact angle values and is depicted in Table S1. Kinetic effects taking place on the wetted surfaces, such as swelling and the reorganization of polymer chains increase the work of adhesion.

Water Flux and Thermoresponsive Behavior. Microgel membranes were subjected to water permeation studies and thermoresponsive behavior to assess their water filtration performance. The data are presented in Figure 4(A and B).

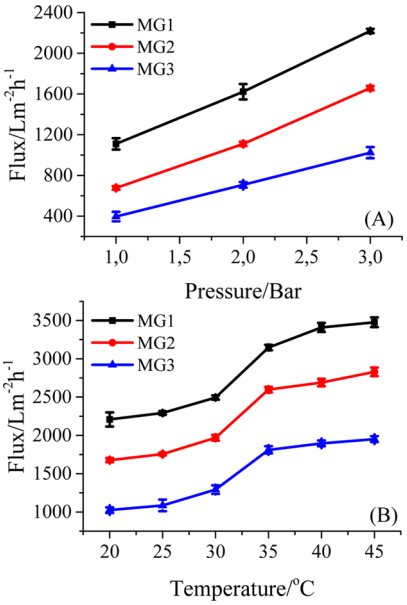

Figure 4. (A) Water flux and (B) thermoresponsive behavior of microgel based cross-linked ultrathin membranes.

The prepared membranes were ultrathin, hydrophilic, and temperature responsive in nature, which facilitates the high water transport under low pressure due to less resistance. The water permeation of membranes was inversely proportional to the thickness of microgel layer. The porosity of the microgel layer on PET membrane was estimated by using Hagen−Poiseuille equation:

$$J_w = \frac{\varepsilon \pi r_p^2}{8\mu\delta\tau}\Delta p \tag{5}$$

where J_w is the volume flux (L m^{-2} s^{-1}), ε is the surface porosity, r_p is the average pore radius (m), μ is the viscosity (Pa s), δ is the thickness (m), τ is the tortuosity, and Δp is the pressure drop across the membrane (Pa).[36] The pore size (r_p) of microgel membranes was calculated, presuming the hexagonal packing of the corresponding microgels using the relationship $r_p = 0.07735 \times D$, where D is the diameter of microgel particles obtained by SEM imaging of microgel particles. The average pore radius of microgel membranes was calculated as 6.2 nm. Based on water flux of microgel membranes, we estimated the surface porosity of the membrane to be in the range 5.1, 4.5, and 3.4% at 20 °C and 8.05, 7.5, and 6.7% at 45 °C for MG-1, MG-2, and MG-3 membranes, respectively. The surface porosity should be no larger than the one obtained from the water content of the hydrated membrane.[37] The surface porosity from water absorption (at RT) was estimated to be 22, 40, and 44% for MG-1, -2, and -3 respectively. The high porosity by water absorption can be described due to the hydrophilic nature of the microgels and association of water molecules with PNIPAm and other constituents. Thus, most of the water molecules were associated with the transition and swelling of PNIPAm chains.

dx.doi.org/10.1021/am504120c | ACS Appl. Mater. Interfaces 2014, 6, 17702−17712

The thermoresponsive nature of the membranes was evaluated by recording the water flux at different temperatures ranging from 20 to 45 °C. A gradual increase in flux was observed at lower temperatures, but a jump can be seen above 32 °C in Figure 4 B. It is clear that the water flux through the temperature-sensitive membrane depends little on the temperature when the temperature is lower than 30 °C. However, when the temperature was higher than 32 °C, the LCST of PNIPAm, water flux increases significantly with the rise of temperature. The pure water flux was increased by a factor of 1.5−2 at 45 °C as compared to 20 °C for all membranes. The collapse of PNIPAm chains and shrinking of microgel particle size (as observed in DLS study) led to the enlargement of voids in microgel packing. This enlargement of voids reduces the resistance for water flow and thus a higher flux was observed at temperatures above 32 °C. To examine reversibility, the repeatability of thermoresponsive "open-close" gating valve of microgel membranes (MG-3) was investigated and the results are shown in Figure S4 (Supporting Information). The water flux was measured at 20 and 45 °C alternatively for repeated five cycles. Almost similar values were obtained for each consecutive cycle which shows good stability and tenability of microgel membrane. Overall, the membrane showed good thermo-response repeatability and can be well regarded as membrane with thermo-switching gates.

Application of Microgel Based Membranes in Different Processes. *Dye Rejection Performance.* The rejection of low molecular weight organic compounds is one of the promising applications of membranes that can be used in many industrial processes and water purification applications. We used the prepared microgel membranes to study the rejection behavior of three selected small molecular weight dyes (the characteristics are given in Table S2, Supporting Information), namely, methylene blue, methyl red, and congo red through MG-3 membrane. The concentration of dye species in feed, permeate, and retentate are estimated with UV−vis spectroscopy and the respective spectra are presented in Figures S5, S6, and S7 (Supporting Information). The rejection and membrane performance data are presented in Figure 5.

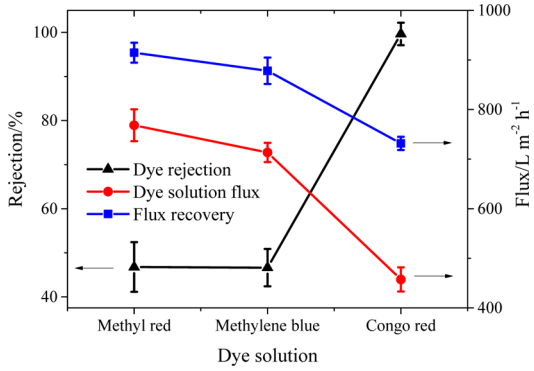

Figure 5. Dye rejection performance with MG-3 microgel membrane.

We estimated the solution flux, rejection efficiency, and flux recovery after thorough cleaning of the membrane. Methyl red and methylene blue rejection was almost similar, and about 46% rejection was observed, while more than 90% rejection was observed in case of congo red. This rejection behavior can be explained by the combined effect of molecular weight, volume, charge nature of dyes, and pore size of the membranes. The low rejection for methyl red and methylene blue was due to the small size and volume of both dye molecules. Almost complete rejection of congo red through MG-3 membrane showed that the cutoff value was below the molecular weight of congo red. The negatively charged nature of the congo red may also play an important role in a high rejection due to donnan exclusion. Congo red also associates and form colloids in water, which led to high rejection during filtration.[38] The flux during dye filtration was also considerably reduced due to adsorption of dye molecules on the membrane surface leading to the reduction in pore size. The maximum reduction in flux was observed during congo red filtration. Congo red adsorption was visually observed on the membrane surface, which can be explained due to the charged nature of congo red. Congo red is an anionic dye and can associate with the PNIPAm moiety of microgel. After dye filtration, membrane was thoroughly washed to remove the adsorbed dye species and water flux was rerecorded. The recovery data are presented in Figure 5 and indicate that about 92, 88, and 74% flux recovery was observed for methyl red, methylene blue, and congo red, respectively. These data indicate that microgel based ultrathin nanostructured membranes can be good candidates for dye removal, separation, and water purification applications.

Protein Separation Performance. The protein rejection performance was studied using lysozyme as a model protein. The lysozyme separation performance data for MG-3 membrane is given in Figure S8 (Supporting Information). The narrow pore size distribution in thin microgel films leads to the almost complete rejection of lysozyme protein with higher fluxes. About 99% rejection and ∼695 L m^{-2} h^{-1} flux was observed for MG-3 membrane at 3 bar pressure. After lysozyme filtration, 72% flux recovery was achieved by thorough cleaning of the membrane. A lysozyme molecule in solution has an almost ellipsoidal shape with dimensions of 2.8 × 3.2 × 3.0 nm and a volume of 2.7 × 10^{-20} cm^3.[39] A large amount of water is also associated with each lysozyme molecule due to hydrogen bonding. PNIPAm surfaces are reported for their protein resistive nature due to the presence of large amounts of water molecules in the vicinity of the hydrophilic part below LCST.[40] Thus, the water molecules on lysozyme and PNIPAm make a resistive layer that hinders the penetration of lysozyme in microgel membranes and their passage through it. The high rejection with good flux and recovery makes these membranes attractive for separation and isolation of proteins and biomolecules.

Synthesis and Immobilization of Gold Nanoparticles for Catalytic Applications. We explored the strategy to grow gold nanoparticles (GNP) into the synthesized microgels because we believed that these microgels, might serve as host to template the growth of gold nanoparticles. The presence of the large number of nitrogen containing groups (amide and amino) in the synthesized microgel enables the complexation of $[AuCl_4]^-$ ions and subsequently the formation of GNP by in situ reduction with $NaBH_4$. Also, the core dissolved microgel may be advantageous in terms of diffusion of $[AuCl_4]^-$ ions into the prepared microgel system. It is reported that in PNIPAm based microgels, the gold nanoparticles formation occur preferentially on the surface due to the disruption of the large number of inter chain hydrogen bonds during the diffusion process.[41] In the present study, the diffusion of ions in hollow microgel may be comparatively easier due to the greater swelling and less cross-linked nature. The synthetic approach of gold nanoparticles in free microgel solution is presented in

Figure S9 (Supporting Information). A similar approach was followed for GNPs synthesis in microgel thin membranes. However, the diffusion of $HAuCl_4$ was carried out under mild applied pressure in the filtration assembly. The diffusion and retention of $[AuCl_4]^-$ ions in PNIPAm-APMA shell is caused by complexation of $[AuCl_4]^-$ ions with nitrogen atoms of PNIPAm, APMA, and BIS. The reduction in both free microgels and in the membrane was done with $NaBH_4$, which could be seen by the darkening color of microgel suspension and the membrane (Figure S10, Supporting Information). The UV absorption spectra of GNP-microgel complex and centrifuged supernatant (Figure S11, Supporting Information) revealed that a small red shift was observed for the gold nanoparticles−microgel (GNP-MG) complex. This red shift can be due to the chemical interactions between GNP and microgel and due to plasmon effect. The supernatant gold nanoparticles showed absorption maxima at 532 while for GNP-MG complex, the maximum was observed at 540 nm. Thus, the nanoparticles in microgels were larger than in the supernatant. Since similar conditions were used to synthesize the gold nanoparticle in the membrane, we assume similar characteristics for gold nanoparticles in the membrane. The morphology of GNP loaded microgels was also characterized by AFM, and the images are presented in Figure S12 (Supporting Information). The images clearly indicate that Au particles were formed on the microgel particles. The microgel particles were covered with small GNPs, and the hollow core was not visible. This may indicate that a large number of GNPs was embedded in microgel particles.

Both, the GNP-MG complex and the membrane were subjected to catalytic reduction of *p*-nitrophenol into *p*-aminophenol in the presence of $NaBH_4$. The reduction reaction with different amounts of GNP-MG complex was performed and monitored in UV cuvette at regular interval. The representative time dependent UV−vis spectra are presented in Figure S13 (Supporting Information). The rapid decrease of the absorption peak at 400 nm and an increase at around 300 nm, showed the conversion of *p*-nitrophenol to *p*-aminophenol, respectively. The data in Figure S13 indicate that the reaction terminates within a time frame of 5−10 min depending upon the amount of GNP-MG. The degree of conversion can be directly read off these spectra, since c_t, the concentration of *p*-nitrophenol at time *t*, can be calculated based on absorbance at 400 nm, and the ratio of c_t to its value c_0 at $t = 0$ can be directly given by the relative intensity of the respective absorbances A_t/A_0.[42] The high excess of $NaBH_4$ ensures that its concentration remains essentially constant during the reaction. Thus, the catalytic rate constant (K) for the reaction can be evaluated by considering pseudo first order kinetics with respect to *p*-nitrophenol concentration.[43−45] The rate constant of the reduction reaction was calculated from the slope of the linear region of natural logarithmic of absorbance data at 400 nm. The data are presented in Figure 6. Rate constants (K) were found to be 0.29×10^{-2} s^{-1}, 0.56×10^{-2} s^{-1}, and 0.97×10^{-2} s^{-1} and 1.18×10^{-2} s^{-1} for reactions with 25, 50, 75, and 100 μL MG-GNP solutions, respectively. The rate constants are proportional to the amount of GNP-microgel solution taken for the reduction reaction. The high rate constant with high catalytic dose can be explained due to increased number of reaction sites. PNIPAm has been widely used to construct thermo responsive support for immobilization of different catalytic nanoparticles such as Pt, Pd, Ag, Au, etc.[44,46−48] It is reported that these catalytic systems exhibit

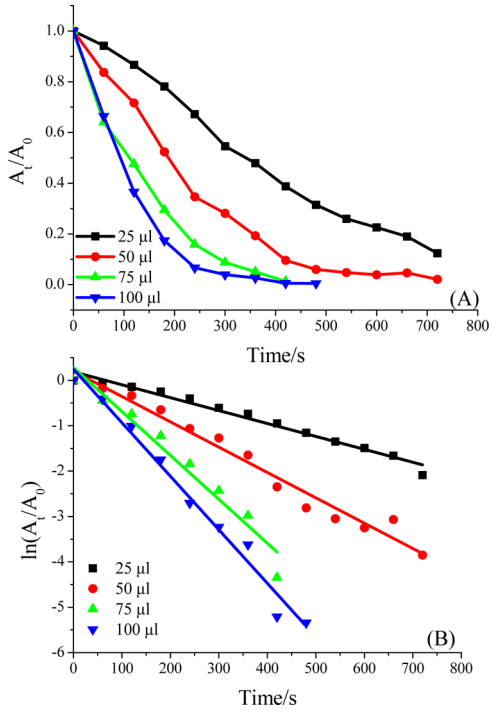

Figure 6. Change in absorbance (A) and their logarithmic plot (B) of the decrease of absorption at 400 nm with time for *p*-nitrophenol reduction reaction with different GNP−microgel concentration.

normal Arrhenius-like behavior and the rate constant increases with temperature.[47] In this study, the presence of PNIPAm and APMA provides both thermo responsive behavior and free amine group for coordination with gold ions/nanoparticles. Thus, a similar behavior can be postulated for the present catalytic system. Also, the hollow nature of the microgels provides additional benefits to accommodate more nanoparticles and diffusion of reactants due to greater swelling.

We also studied the catalytic performance of GNP−microgel composite membrane in stirred cell reactor under different applied pressure or flux condition. The data presented in Figure 7(A−D), indicate that the reduction of *p*-nitrophenol in the membrane reactor largely depends upon the residence time. Low reduction was observed at high filtration pressure (3 bar) or flux condition, whereas almost 100% conversion can be seen at low pressure (1 bar). The photograph of the membrane reactor setup and reaction is depicted in Figure S14 (Supporting Information). The data in Figure 7C also indicate a linear relation between conversion of *p*-nitrophenol to aminophenol and flux value. Almost 100% conversion at sufficient high fluxes indicates that the prepared membrane can be used for such chemical conversion reactions. We also studied the long-term stability and performance of GNP-microgel composite membrane by performing the catalytic conversion for 10 continuous cycles. After each cycle, the membrane was properly cleaned with water. The data presented in Figure 7D indicates that the activity of prepared membrane was almost unchanged. This indicates that the prepared membrane can be used for long-term application without compromising the catalytic performance. A possible application of these membranes can be in azo dye reduction/degradation for water treatment applications.

Immobilization of Enzyme for Biocatalytic Applications. Microgels are believed to be suitable support material for

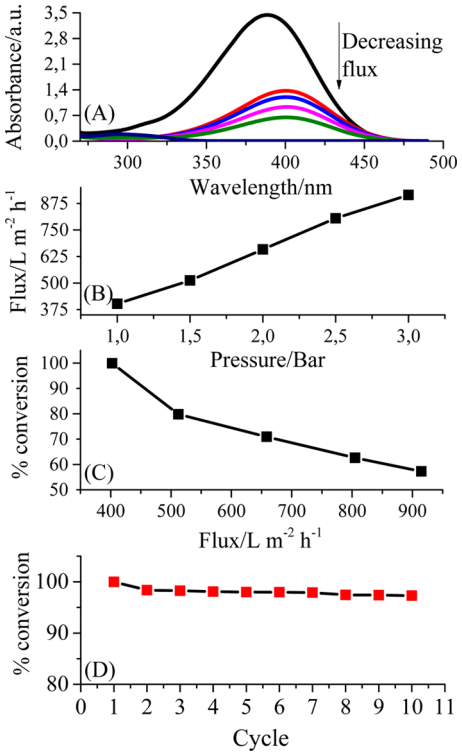

Figure 7. Catalytic performance of gold nanoparticle−microgel composite membrane: (A) UV absorbance of permeate under different applied pressure; (B) flux vs pressure of composite membrane; (C) % conversion of *p*-nitrophenol to aminophenol at different pressure/flux, and (D) % conversion of *p*-nitrophenol to aminophenol at 400 L m^{-2} h^{-1} for consecutive 10 cycles.

immobilization and anchoring of biomolecules for various biochemical processes due to the flexibility in tuning the structure and charge properties.[49,50] Since the present membrane was formed with an ultrathin layer of microgel, we studied the immobilization of lactate dehydrogenase (LDH) enzyme and its use to catalyze pyruvate to lactate reaction. LDH was covalently cross-linked on the microgel membrane surface via glutaraldehyde, and 101.8 μg cm^{-2} immobilization was calculated. The enzyme immobilization conditions are given in Table S3 (Supporting Information). The immobilization of LDH was quite firm and stable under continuous repeated washing. The UV absorbance spectra of original and repeated wash solution are depicted in Figure S15 (Supporting Information). In the third wash cycle, almost no LDH was observed in the permeate, which confirmed that the bonding was stable. The membrane showed a flux loss after the immobilization of LDH on the membrane, which is within expected lines (Figure S16, Supporting Information). The conversion rate was determined by monitoring the NADH concentration in permeate. The high value of conversion rate reflects that the time required to travel through the membrane was sufficient for the reaction to happen. This conversion rate also indicates that the enzyme molecules maintained their activity after the immobilization on the membrane surface. The reaction of pyruvate to lactate formation is given below in Scheme 1.

The linear rate of conversion of NADH showed the stable and active nature of immobilized enzyme on the membrane surface. Figure 8 revealed that more than 65% conversion was observed in the first 1 h of reaction. Also, the membrane

Scheme 1. Reaction Scheme of Pyruvate to Lactate Conversion

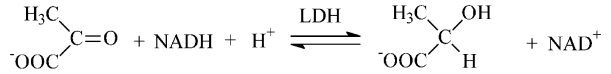

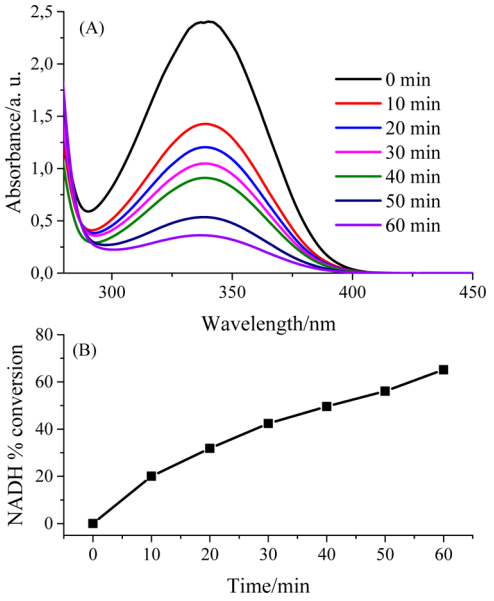

Figure 8. Conversion of NADH into NAD^+ showing the formation of lactate from pyruvate in catalytic membrane reactor under flow through condition with time: (A) UV−vis spectra of permeate at different time interval, and (B) percent conversion of NADH.

retained its catalytic activity after the first cycle and no prominent change was observed for three consecutive cycles of operation. The above observations confirmed that the prepared ultrathin microgel based membranes can be used to immobilize biomolecules for biochemical conversions and reactions.

CONCLUSIONS

We report the use of microgel-based soft, thin films to construct ultrathin responsive membranes in an easy and straightforward way for separation, and catalytic applications. The microgels were synthesized in core−shell manner, and the core was removed by selective degradation of its constituent. These hollow microgels were transformed into an ultrathin film by suction filtration and cross-linking over $Cd(OH)_2$ nanostrand sacrificial layer. The prepared membranes were characterized for structure, morphology, hydrophilic property, and membrane performance. The prepared membranes were tested for water purification, dye rejection, protein separation, and gold nanoparticle and enzyme immobilization for catalytic application. High water flux and rejection of small molecular weight dyes with thermoresponsive character indicates that these ultrathin membranes can be used for water purification applications. High rejection of protein and flux recovery showed their separation and antifouling abilities for bioseparation and isolations. The in situ synthesis and stability of gold nanoparticles in membranes as well as in free microgels lead to the formation of catalytically active membranes, which can be used in many chemical transformation processes. The covalent immobilization and the retained activity of lactate dehydrogenase indicate its suitability for biochemical processes. Thus, the prepared microgel membrane performed very well in all these

applications and the idea can be extrapolated to other soft matter and microgels as well. The possibility to immobilize metal nanoparticles, biocatalysts, etc. indicates the applicability in a wide range of applications.

■ ASSOCIATED CONTENT

Supporting Information

Dynamic light scattering data of the core and core−shell microgels, microgel degradation pictures, SEM and AFM images of microgels, temperature response hysteresis, properties of membranes, chemical structure and characteristics of different dyes used for rejection performance, UV−vis spectra of dye and protein rejection, schematic of gold nanoparticle synthesis, pictures of gold nanoparticles in solution and on the membrane, UV spectra of gold nanoparticles, AFM images of gold nanoparticle immobilized microgels, UV spectra of *p*-nitrophenol reduction, picture of stirred cell showing reduction of *p*-nitrophenol, and data for LDH immobilization. This material is available free of charge via the Internet at http://pubs.acs.org.

■ AUTHOR INFORMATION

Corresponding Authors

*Fax: +49-3514658281. Tel: +49-3514658326. Email: bijayptripathi@yahoo.com, tripathi@ipfdd.de.
*Email: stamm@ipfdd.de.

Author Contributions

The manuscript was written through contributions of all authors. All authors have given approval to the final version of the manuscript.

Notes

The authors declare no competing financial interest.

■ REFERENCES

(1) Funke, W.; Okay, O.; Joos-Müller, B. Microgels Intramolecularly Crosslinked Macromolecules with a Globular Structure. In *Microencapsulation Microgels Iniferters*; DiMari, S.; Funke, W.; Haralson, M. A.; Hunkeler, D.; Joos-Müller, B.; Matsumoto, A.; Okay, O.; Otsu, T.; Powers, A. C.; Prokop, A.; Wang, T. G.; Whitesell, R. R., Eds.; Springer: Berlin Heidelberg, 1998; Chapter 4, pp 139−234.
(2) Heyes, D. M.; Branka, A. C. Interactions between Microgel Particles. *Soft Matter* **2009**, *5*, 2681−2685.
(3) Di Lorenzo, F.; Seiffert, S. Macro- and Microrheology of Heterogeneous Microgel Packings. *Macromolecules* **2013**, *46*, 1962−1972.
(4) Jones, C. D.; Lyon, L. A. Synthesis and Characterization of Multiresponsive Core−Shell Microgels. *Macromolecules* **2000**, *33*, 8301−8306.
(5) Pelton, R. Temperature-Sensitive Aqueous Microgels. *Adv. Colloid Interface Sci.* **2000**, *85*, 1−33.
(6) Pelton, R.; Hoare, T. (2011) Microgels and Their Synthesis: An Introduction. In *Microgel Suspensions*. Eds: Fernandez-Nieves, A.; Wyss, H. M.; Mattsson, J.; Weitz, D. A. Wiley-VCH Verlag GmbH & Co. KGaA: Weinheim, Germany; pp. 1−32.
(7) Jeong, B.; Bae, Y. H.; Lee, D. S.; Kim, S. W. Biodegradable Block Copolymers as Injectable Drug-Delivery Systems. *Nature* **1997**, *388*, 860−862.
(8) Lyon, L. A.; Fernandez-Nieves, A. The Polymer/Colloid Duality of Microgel Suspensions. *Annu. Rev. Phys. Chem.* **2012**, *63*, 25−43.
(9) Hellweg, T. Responsive Core−Shell Microgels: Synthesis, Characterization, and Possible Applications. *J. Polym. Sci., Part B: Polym. Phys.* **2013**, *51*, 1073−1083.
(10) Schmidt, S.; Zeiser, M.; Hellweg, T.; Duschl, C.; Fery, A.; Möhwald, H. Adhesion and Mechanical Properties of PNIPAM Microgel Films and their Potential use as Switchable Cell Culture Substrates. *Adv. Funct. Mater.* **2010**, *20*, 3235−3243.
(11) Vogel, N.; Fernández-López, C.; Pérez-Juste, J.; Liz-Marzán, L. M.; Landfester, K.; Weiss, C. K. Ordered Arrays of Gold Nanostructures from Interfacially Assembled Au@PNIPAM Hybrid Nanoparticles. *Langmuir* **2012**, *28*, 8985−8993.
(12) Richtering, W.; Pich, A. The Special Behaviours of Responsive Core−Shell Nanogels. *Soft Matter* **2012**, *8*, 11423−11430.
(13) X, W.; X, Q.; C, W. Comparison of the Coil-to-Globule and the Globule-to-Coil Transitions of a Single Poly(N-isopropylacrylamide) Homopolymer Chain in Water. *Macromolecules* **1998**, *31*, 2972−2976.
(14) Philipp, M.; Kyriakos, K.; Silvi, L.; Lohstroh, W.; Petry, W.; Krüger, J. K.; Papadakis, C. M.; Müller-Buschbaum, P. From Molecular Dehydration to Excess Volumes of Phase-Separating PNIPAM Solutions. *J. Phys. Chem. B* **2014**, *118*, 4253−4260.
(15) Spears, M. W.; Herman, E. S.; Gaulding, J. C.; Lyon, L. A. Dynamic Materials from Microgel Multilayers. *Langmuir* **2014**, *30*, 6314−6323.
(16) Nolan, C. M.; Reyes, C. D.; Debord, J. D.; García, A. J.; Lyon, L. A. Phase Transition Behavior, Protein Adsorption, and Cell Adhesion Resistance of Poly(ethylene glycol) Cross-Linked Microgel Particles. *Biomacromolecules* **2005**, *6*, 2032−2039.
(17) Schwartz, V. B.; Thétiot, F.; Ritz, S.; Pütz, S.; Choritz, L.; Lappas, A.; Förch, R.; Landfester, K.; Jonas, U. Antibacterial Surface Coatings from Zinc Oxide Nanoparticles Embedded in Poly(N-isopropylacrylamide) Hydrogel Surface Layers. *Adv. Funct. Mater.* **2012**, *22*, 2376−2386.
(18) Valade, D.; Wong, L. K.; Jeon, Y.; Jia, Z.; Monteiro, M. J. Polyacrylamide Hydrogel Membranes with Controlled Pore Sizes. *J. Polym. Sci., Part A: Polym. Chem.* **2013**, *51*, 129−138.
(19) Yang, Q.; Adrus, N.; Tomicki, F.; Ulbricht, M. Composites of Functional Polymeric Hydrogels and Porous Membranes. *J. Mater. Chem.* **2011**, *21*, 2783−2811.
(20) Arıca, M. Y.; Bayramoğlu, G.; Arıca, B.; Yalçın, E.; Ito, K.; Yagci, Y. Novel Hydrogel Membrane Based on Copoly(hydroxyethyl methacrylate/*p*-vinylbenzyl-poly(ethylene oxide)) for Biomedical Applications: Properties and Drug Release Characteristics. *Macromol. Biosci.* **2005**, *5*, 983−992.
(21) Tang, M.; Zhang, R.; Bowyer, A.; Eisenthal, R.; Hubble, J. A Reversible Hydrogel Membrane for Controlling the Delivery of Macromolecules. *Biotechnol. Bioeng.* **2003**, *82*, 47−53.
(22) Zhou, J.; Childs, R. F.; Mika, A. M. Calculation of the Salt Separation by Negatively Charged Gel-Filled Membranes. *J. Membr. Sci.* **2005**, *260*, 164−173.
(23) Zhou, J.; Childs, R. F.; Mika, A. M. Pore-Filled Nanofiltration Membranes Based on Poly(2-acrylamido-2-methylpropanesulfonic acid) Gels. *J. Membr. Sci.* **2005**, *254*, 89−99.
(24) Ainseba-Chirani, N.; Dembahri, Z.; Tokarski, C.; Rolando, C.; Benmouna, M. Newly Designed Polyacrylamide/Dextran Gels for Electrophoresis Protein Separation: Synthesis and Characterization. *Polym. Int.* **2011**, *60*, 1024−1029.
(25) Yang, J. M.; Su, W. Y.; Leu, T. L.; Yang, M. C. Evaluation of Chitosan/PVA Blended Hydrogel Membranes. *J. Membr. Sci.* **2004**, *236*, 39−51.
(26) Monteiro, M. J.; Hall, G.; Gee, S.; Xie, L. Protein Transfer through Polyacrylamide Hydrogel Membranes Polymerized in Lyotropic Phases. *Biomacromolecules* **2004**, *5*, 1637−1641.
(27) Rylatt, D. B.; Napoli, M.; Ogle, D.; Gilbert, A.; Lim, S.; Nair, C. H. Electrophoretic Transfer of Proteins Across Polyacrylamide Membranes. *J. Chromatogr. A* **1999**, *865*, 145−153.
(28) Singh, N.; Bridges, A. W.; García, A. J.; Lyon, L. A. Covalent Tethering of Functional Microgel Films onto Poly(ethylene terephthalate) Surfaces. *Biomacromolecules* **2007**, *8*, 3271−3275.
(29) Baker, R. W. Front Matter. In *Membrane Technology and Applications*; John Wiley & Sons, Ltd: 2004; pp i−xiii.
(30) Nayak, S.; Gan, D.; Serpe, M. J.; Lyon, L. A. Hollow Thermoresponsive Microgels. *Small* **2005**, *1*, 416−421.

(31) Ichinose, I.; Kurashima, K.; Kunitake, T. Spontaneous Formation of Cadmium Hydroxide Nanostrands in Water. *J. Am. Chem. Soc.* **2004**, *126*, 7162−7163.
(32) Tripathi, B. P.; Dubey, N. C.; Choudhury, S.; Stamm, M. Antifouling and Tunable Amino Functionalized Porous Membranes for Filtration Applications. *J. Mater. Chem.* **2012**, *22*, 19981−19992.
(33) Xu, J.; Zeng, F.; Wu, S.; Liu, X.; Hou, C.; Tong, Z. Gold Nanoparticles Bound on Microgel Particles and their Application as an Enzyme Support. *Nanotechnol.* **2007**, *18*, 265704−265712.
(34) Lyon, L. A.; Meng, Z.; Singh, N.; Sorrell, C. D.; St. John, A. Thermoresponsive Microgel-Based Materials. *Chem. Soc. Rev.* **2009**, *38*, 865−874.
(35) Nayak, S.; Lyon, L. A. Soft Nanotechnology with Soft Nanoparticles. *Angew. Chem., Int. Ed.* **2005**, *44*, 7686−7708.
(36) Wang, Q.; Samitsu, S.; Ichinose, I. Ultrafiltration Membranes Composed of Highly Cross-Linked Cationic Polymer Gel: The Network Structure and Superior Separation Performance. *Adv. Mater.* **2011**, *23*, 2004−2008.
(37) Peng, X.; Jin, J.; Nakamura, Y.; Ohno, T.; Ichinose, I. Ultrafast Permeation of Water through Protein-Based Membranes. *Nat. Nanotechnol.* **2009**, *4*, 353−357.
(38) Tripathi, B. P.; Dubey, N. C.; Stamm, M. Functional Polyelectrolyte Multilayer Membranes for Water Purification Applications. *J. Hazard. Mater.* **2013**, *252*−*253*, 401−412.
(39) Steinrauf, L. Preliminary X-ray Data for Some New Crystalline Forms of β-Lactoglobulin and Hen-Egg-White Lysozyme. *Acta Crystallogr.* **1959**, *12*, 77−79.
(40) Burkert, S.; Bittrich, E.; Kuntzsch, M.; Muller, M.; Eichhorn, K. J.; Bellmann, C.; Uhlmann, P.; Stamm, M. Protein Resistance of Pnipaam Brushes: Application to Switchable Protein Adsorption. *Langmuir* **2010**, *26*, 1786−1795.
(41) Kim, J.-H.; Lee, T. R. Hydrogel-Templated Growth of Large Gold Nanoparticles: Synthesis of Thermally Responsive Hydrogel−Nanoparticle Composites. *Langmuir* **2007**, *23*, 6504−6509.
(42) Zhu, C. H.; Hai, Z. B.; Cui, C. H.; Li, H. H.; Chen, J. F.; Yu, S. H. In Situ Controlled Synthesis of Thermosensitive Poly(N-isopropylacrylamide)/Au Nanocomposite Hydrogels by γ Radiation for Catalytic Application. *Small* **2012**, *8*, 930−936.
(43) Gangula, A.; Podila, R.; M, R.; Karanam, L.; Janardhana, C.; Rao, A. M. Catalytic Reduction of 4-Nitrophenol using Biogenic Gold and Silver Nanoparticles Derived from Breynia Rhamnoides. *Langmuir* **2011**, *27*, 15268−15274.
(44) Koenig, M.; Simon, F.; Formanek, P.; Müller, M.; Gupta, S.; Stamm, M.; Uhlmann, P. Catalytically Active Nanocomposites Based on Palladium and Platinum Nanoparticles in Poly(2-vinylpyridine) Brushes. *Macromol. Chem. Phys.* **2013**, *214*, 2301−2311.
(45) Wu, S.; Dzubiella, J.; Kaiser, J.; Drechsler, M.; Guo, X.; Ballauff, M.; Lu, Y. Thermosensitive Au-PNIPA Yolk−Shell Nanoparticles with Tunable Selectivity for Catalysis. *Angew. Chem., Int. Ed.* **2012**, *51*, 2229−2233.
(46) Horecha, M.; Kaul, E.; Horechyy, A.; Stamm, M. Polymer Microcapsules Loaded with Ag Nanocatalyst as Active Microreactors. *J. Mater. Chem. A* **2014**, *2*, 7431−7438.
(47) Koenig, M.; Magerl, D.; Philipp, M.; Eichhorn, K.-J.; Müller, M.; Müller-Buschbaum, P.; Stamm, M.; Uhlmann, P. Nanocomposite Coatings With Stimuli-Responsive Catalytic Activity. *RSC Adv.* **2014**, *4*, 17579−17586.
(48) Herves, P.; Perez-Lorenzo, M.; Liz-Marzan, L. M.; Dzubiella, J.; Lu, Y.; Ballauff, M. Catalysis by Metallic Nanoparticles in Aqueous Solution: Model Reactions. *Chem. Soc. Rev.* **2012**, *41*, 5577−5587.
(49) Dubey, N. C.; Tripathi, B. P.; Stamm, M.; Ionov, L. Smart Core−Shell Microgel Support for Acetyl Coenzyme A Synthetase: A Step Toward Efficient Synthesis of Polyketide-Based Drugs. *Biomacromolecules* **2014**, *15*, 2776−2783.
(50) Wiese, S.; Spiess, A. C.; Richtering, W. Microgel-Stabilized Smart Emulsions for Biocatalysis. *Angew. Chem., Int. Ed.* **2013**, *52*, 576−579.